MoiréWidgets: High-Precision, Passive Tangible Interfaces via Moiré Effect

Daniel Campos Zamora
danielcz@cs.uw.edu
University of Washington
Seattle, WA, USA

Mustafa Doga Dogan
doga@mit.edu
MIT CSAIL
Cambridge, MA, USA

Alexa Siu
asiu@adobe.com
Adobe Research
San Jose, CA, USA

Eunyee Koh
eunyee@adobe.com
Adobe Research
San Jose, CA, USA

Chang Xiao
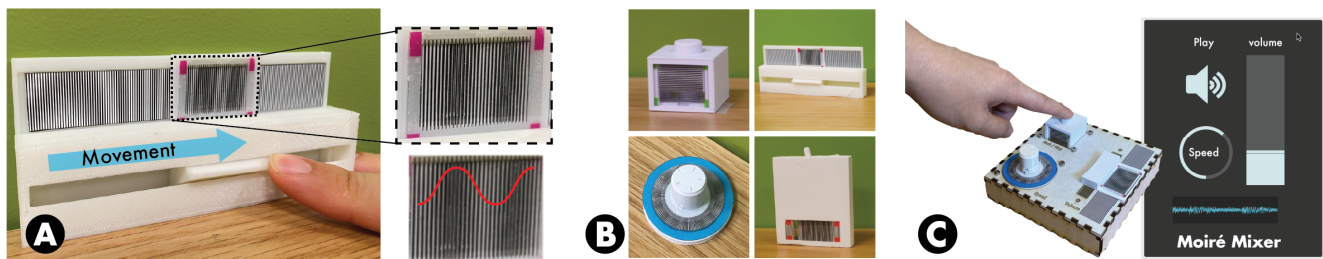cxiao@adobe.com
Adobe Research
San Jose, CA, USA

Figure 1: MoiréWidgets offer high-precision event detection on passive physical controls by using the Moiré effect to detect subtle input movements. Our image processing pipeline (A) extracts the Moiré pattern from the widget and calculates the displacement from the phase shift of the fringes as the user moves a slider. We use this approach to develop a set of controls (B) buttons, sliders, dials, and switches made using a two-step fabrication approach with 3D printed mechanical structures and paper printed fringes. We demonstrate how multiple widgets can be combined to create (C) a physical audio console.

ABSTRACT

We introduce MoiréWidgets, a novel approach for tangible interaction that harnesses the Moiré effect—a prevalent optical phenomenon—to enable high-precision event detection on physical widgets. Unlike other electronics-free tangible user interfaces which require close coupling with external hardware, MoiréWidgets can be used at greater distances while maintaining high-resolution sensing of interactions. We define a set of interaction primitives, e.g., buttons, sliders, and dials, which can be used as standalone objects or combined to build complex physical controls. These consist of 3D printed structural mechanisms with patterns printed on two layers—one on paper and the other on a plastic transparency sheet—which create a visual signal that amplifies subtle movements, enabling the detection of user inputs. Our technical evaluation shows that our method outperforms standard fiducial markers and maintains sub-millimeter accuracy at 100 cm distance and wide viewing angles. We demonstrate our approach by creating an audio console and indicate how our approach could extend to other domains.

CCS CONCEPTS

• **Human-centered computing** → **Human computer interaction (HCI)**.

KEYWORDS

Moiré Effect, Moiré Pattern, Fabrication, Tangible Interaction, Vision-Based Sensing

1 INTRODUCTION

Tangible user interfaces (TUIs) provide tactile and proprioceptive feedback which improves task comprehension, speed, and precision, making them well-suited for a wide breadth of applications including education, gaming, and data visualization [23, 28]. Typically, they rely on embedded circuits that need power to function and software/hardware expertise to create. This makes them difficult to maintain and complex to produce [20].

Consequently, there has been significant interest in electronics-free approaches to sense interactions. For example, researchers have built *passive* systems to detect changes in the magnetic field [25, 26], air pressure [21], IMU signals [56], touch [7], and sound [30] to

Daniel Campos Zamora, Mustafa Doga Dogan, Alexa Siu, Eunyee Koh, and Chang Xiao

register inputs. Among these passive channels, vision-based sensing offers an untethered, uniform mechanism that is compatible with a wide variety of devices equipped with cameras. Typically, vision-based methods incorporate fiducial markers to observe marker displacement and harness image data as an input signal. Such methods often face challenges in detection accuracy, as marker detection can be influenced by various factors, including camera distance and viewing angle. To enhance this approach and develop a *more robust and sensitive* vision-based sensing mechanism, we leverage the *Moiré effect*—a visual phenomenon that *amplifies* movement when two periodic patterns are superimposed. We use this ability to detect subtle motions to create passive TUIs ideal for precision controls for AR/VR, robotics, and data visualization.

In this paper, we introduce MoiréWidgets, a novel vision-based TUI that integrates visual features into 3D printed widgets for **high-precision sensing** of interactions via the Moiré effect[1]. Through a combination of 3D printed mechanisms that convert user inputs into basic movements—1D translation, 2D translation, and rotation—and patterns printed on paper, we form Moiré patterns responsive to subtle user movements. Our evaluation shows sub-millimeter accuracy at a meter-long distance and better performance than the commonly used ArUco markers [13, 40]. We recreate popular physical controllers like an audio console to demonstrate our vision-based approach to TUIs.

In summary, this work contributes a vision-based TUI that enables high-precision tracking of passive widgets sensitive to **subtle movements during user interactions** via the Moiré effect with **improved accuracy at various distances and viewing angles** over standard fiducial markers.

2 RELATED WORK

We build on prior research on passive TUIs, vision-based tangible interaction, and applications of the Moiré effect.

2.1 Passive Tangible User Interfaces

Interest in electronics-free TUIs has grown because they are simpler to produce, easier to maintain, and less harmful to the environment [20, 22]. Researchers have explored diverse mechanisms to generate, modulate, and communicate signals from a user to the system [5]. One common approach is to use conductive materials to make objects that sense touch, stretch, and movement [1, 7, 8, 16, 32, 47]. However, these systems depend on wired connections to specialized hardware like micro-controllers with analog-to-digital converters to interpret inputs.

To avoid this dependence on specialized hardware, researchers have used acoustic sensing and microphones to design interactive objects. These objects produce distinct acoustic signals in response to internal resonance [43], mechanical vibrations [42], or pressure changes [21, 30]. These approaches though, are significantly limited in the number of simultaneous interactions they can support due to noise that drowns out user inputs.

Another option is to exploit smartphone sensors like magnetometers [25, 39], IMUs [56], and touchscreens [18, 19, 48] to detect

interactions on external widgets. Although more flexible than hard-wired systems, this approach still has a limited working range since it requires a phone to be embedded within [31], in direct contact with [48], or in close proximity to the widgets [25]. In contrast, Iyer et al. [26] achieve room-scale sensing of 3D printed objects using RF backscatter communication to detect interaction events on the widgets. While these RFID techniques show promise, the resolution is low, sensing is not continuous, and the systems require complex transmitter/receiver setups [33].

2.2 Vision-Based Tracking for Interaction

Researchers in tangible interfaces has long recognized the potential for Computer Vision (CV) to support electronics-free tangible interactions. Early work [29] combined CV with RFID tags to prototype interactions with various physical objects. *SlapWidgets* [54] and *reacTIVision* [27] use a camera and projector setup to track tangibles on interactive surfaces. These systems could only track objects on dedicated work surfaces and had to employ additional mechanisms to register interactions. More closely related to our work is *Sauron* [41], which enables single-camera sensing on physical interfaces by embedding the camera inside the objects. Similarly, *ClipWidgets* [53] is a modular TUI that clips onto a smartphone and uses the back-facing camera to track 3D printed markers. Yet, embedding the cameras within the device limits the working range and requires complex mirror assemblies to track the inputs.

A key strength of vision-based interaction is the ability to track untethered, freely movable objects. Fiducial markers, such as *QR* codes, *ArUco* markers [40], and *AprilTag* [35], can be affixed to 3D printed objects [50, 51] or other physical objects [17, 46, 59] to track interactions. However, these rely on predefined dictionaries of tags which are hard to customize and adapt to complex 3D objects. Some researchers have focused on embedding less obtrusive markers during fabrication to enable object tracking without impacting aesthetics [10, 11, 14, 37]. However, this often requires special lighting conditions or image sensors (i.e., near-infrared cameras) to track the tags. Moreover, occlusion remains a crucial limitation for vison-based systems since they fail when the markers are covered. Researchers have circumvented this issue by using mirrors to see around occluding objects [41] and using additional sensors [52]. Despite these trade-offs, our vision-based method could be a useful addition to passive, battery-free techniques for tangible interaction.

2.3 Applications of Moiré Pattern Interference

The Moiré effect describes the light-dark-light pattern that emerges when two, dense, repetitive patterns are overlaid on one another. This phenomenon can be observed, for instance, when two fine-mesh fabrics slide past each other. Prior work has demonstrated that it is highly sensitive to positional changes [12, 55] making it an excellent candidate for use in high-precision domains like micro-robotics and optics [3].

Lately, there has been a surge in applications utilizing the Moiré effect for camera pose estimation [38, 57]. This is typically done by having two static Moiré patterns with a gap between them, this distance between the layers generates a Moiré effect when viewed from different angles. Harnessing the Moiré effect for *passive tangible interaction* however, remains a largely unexplored area. In a recent demonstration, Zhang et al. [58] developed a silicone

---

[1]Due to image resizing and compression, the Moiré patterns displayed in the paper's figures may not represent their actual appearance in reality. We recommend that readers zoom in when inspecting a Moiré pattern for a better viewing experience.
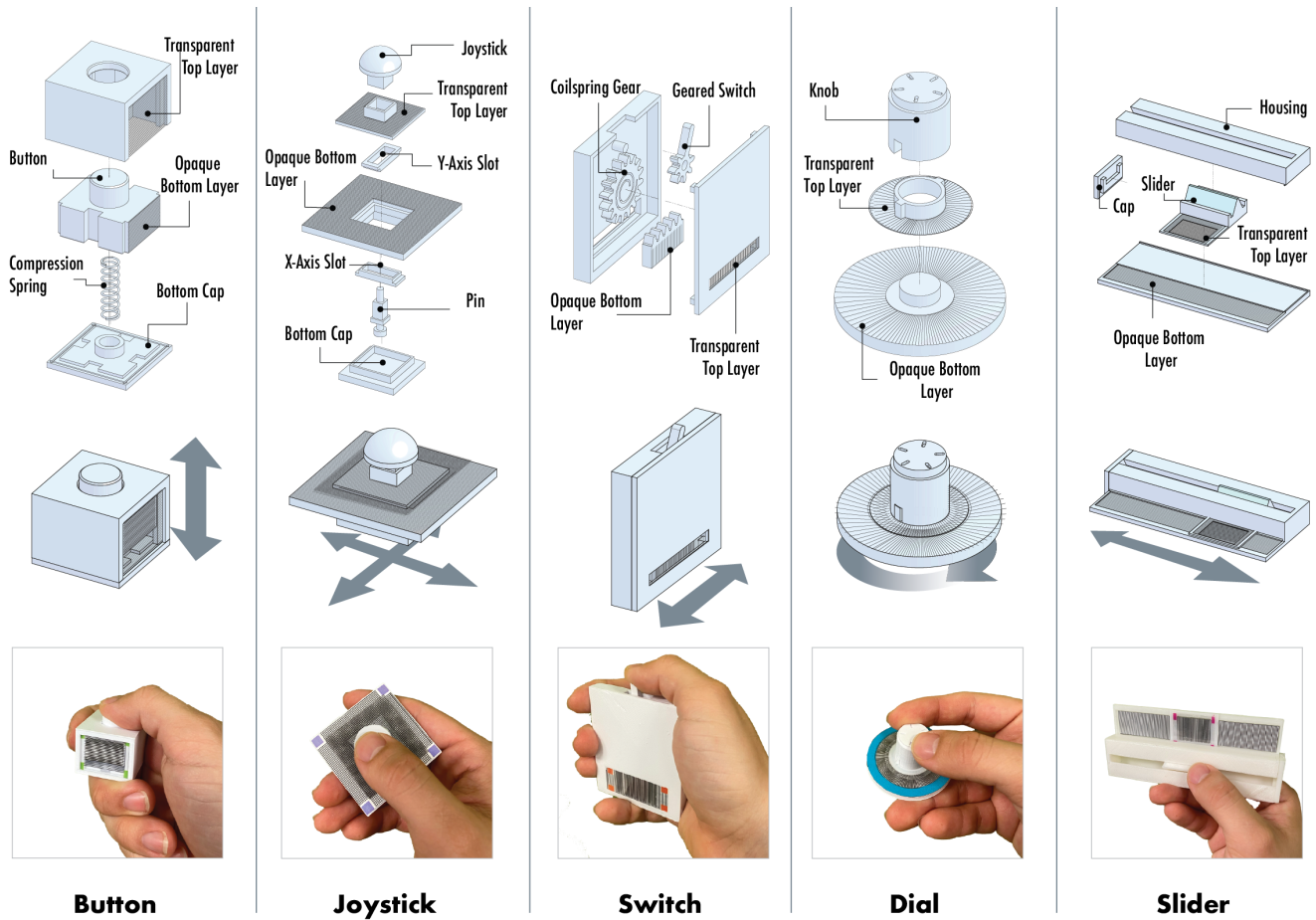
Figure 2: Our MoiréWidgets is composed of 3D printed mechanical structures and paper printed fringes to generate the Moiré effect. We use the printed paper to add color markers to aid our image processing pipeline. This figure shows breakdown of the 3D printed mechanical structures to convert user inputs into the 3 primitive movement types and how the widgets look once they have been assembled.

finger-worn device with fringes to calculate force in touch interactions using the Moiré effect. We aim to leverage the Moiré effect in new ways for multiple inputs on standalone widgets where the Moiré fringes move past each other, thereby enhancing the capabilities for tangible interaction.

3 MOIRÉWIDGETS

MoiréWidgets are set of tangible widgets that generate an amplified visual signal in response to user interaction using Moiré patterns. This section outlines the technical framework of MoiréWidgets by introducing the core operating principle of our approach, the primitive movements that we track, and the mechanisms we use to translate user inputs into respective movement types.

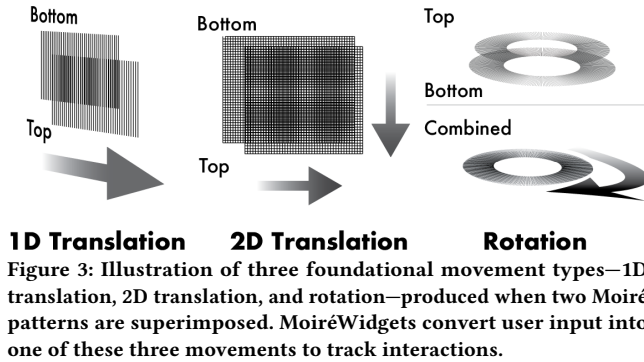### 3.1 Background of Moiré Effect

When two square waves of marginally varied frequencies overlap multiplicatively, the outcome is a combined wave of diverse frequencies called a Moiré pattern. This includes a low base frequency that amplifies and captures the differential positioning of the two

signals. The computational theory of the Moiré Effect has been well studied in earlier research [36, 38, 57, 58]. When two periodic stripe patterns are superimposed without any intervening space, the period of the Moiré fringes, T_m, is solely influenced by the periods of the individual patterns T_a and T_b. It is given by the relation $T_m = \frac{T_a T_b}{T_a - T_b}$. Consequently, a subtle displacement, Δ_b, in the upper layer (assuming the bottom layer is fixed) leads to a displacement in the Moiré fringes, represented as $\Delta_m = \frac{T_a \Delta_b}{T_a - T_b}$. This phenomenon is illustrated in Figure 3.

As demonstrated in the formula, the Moiré effect amplifies the displacement occurring on the top layer. This amplified signal can be harnessed to detect subtle input events from users. In the next section, we identify three basic movements types that use the Moiré effect and illustrate how to implement them on tangible interfaces.

3.2 Primitive Movement Types

We leverage the Moiré effect to amplify three primitive movements—1D translation, 2D translation, and rotation—illustrated in Figure 3 which serve as the foundation for our widgets.

Daniel Campos Zamora, Mustafa Doga Dogan, Alexa Siu, Eunyee Koh, and Chang Xiao

Figure 3: Illustration of three foundational movement types—1D translation, 2D translation, and rotation—produced when two Moiré patterns are superimposed. MoiréWidgets convert user input into one of these three movements to track interactions.

1D Translation. The simplest movement consists of two layers of thin parallel lines with different spacing, or periods, that move along a single axis. Movements orthogonal to the parallel lines generate a visual signal of lower frequency but with higher sensitivity to the displacement. Sliders, buttons, and switches can be decomposed to a 1D movement since they require motion along a single axis.

2D Translation. We can extend the previous movement to two dimensions by creating two grids of perpendicular lines with varying periods. Translation movements along the XY plane will generate a signal that appears like a larger grid. This design can be used for creating thumb-slide joysticks that glide across a plane.

Rotation. Rotational movement requires two concentric patterns of lines with different angular offsets. A shift in the relation between one Moiré pattern to the other yields an altered radial pattern that corresponds to the degree of rotational displacement. This type of design is naturally well-suited for creating dials.

3.3 Widgets Fabrication and Assembly

MoiréWidgets require narrow line features to generate a robust visual signal that can be detected reliably by the camera. According to the theory of Moiré effect [45], the smaller the difference between the two periods of fringe layers, the stronger the signal of the Moiré pattern will be. Our empirical tests have shown that that a difference of 0.05 mm generated a salient visual signal for line widths ranging from 0.25 to 0.4 mm.

Consumer-grade 3D printers lack the precision and consistency to generate reliable Moiré patterns since these fringes are prone to distortion due to issues like under/over extrusion, misalignment, and poor bed adhesion. To address this, we adopted a two-set fabrication approach where we utilize 3D printing for the mechanical assemblies and use a laser paper printer to print the Moiré fringes. Notably, most consumer-grade paper printer can achieve fine details up to a level of 0.02 mm, which meets the requirements for our purpose. In the subsequent paragraph, we outlined the steps of our approach, including 1) 3D printing of the structural components, and 2) the printing and installation of the paper Moiré fringes.

#1: 3D Printing: We use fused deposition modeling (FDM) 3D printing for creating the mechanical structures of our widgets to perform the primitive movements outlined previously. We use standard 3D printing PLA material since it can be printed at lower temperatures to reduce the possibility of warping. Figure 2 illustrates the

3D printed mechanical structures to convert user inputs to planar movements that can be easily detected. Some widgets incorporate springs to help reset the position of a button or switch.

#2: Integration of Moiré pattern and assembly: The Moiré patterns themselves are not 3D printed but are instead printed using a laser printer. The paper with Moiré patterns is then integrated into the 3D printed structures, which ensures that the Moiré patterns remain stable during user interactions. The top transparent layers are printed on transparent sheets and placed into "window" features in the 3D structures. The bottom opaque layer is printed on sticker paper with an adhesive backing and attached directly onto the 3D printed components. We also use the laser printer to print color markers at the corners of the Moiré fringes which is used for our image processing pipeline described in the next section. Figure 2 shows all the assembled widgets and how they may be used.
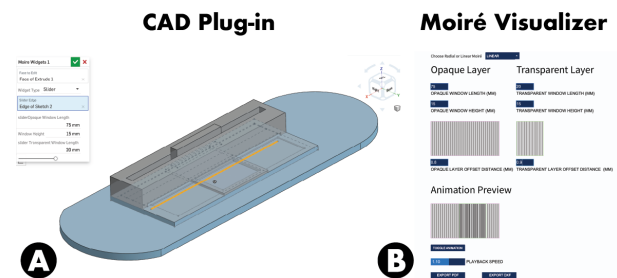

Figure 4: Our two design tools aid in the creation of 3D mechanical structures and paper-printed Moiré fringes for the widgets. (A) Our *OnShape* feature embeds the widgets' mechanical components into 3D models. (B) Our GUI allows users to size, preview, and export linear and radial Moiré patterns which can be printed on paper and inserted into the 3D printed widgets.

3.4 Software Support Tools and Design Guidelines

To facilitate the design process, we developed a set of software tools to assist with the two key aspects of our implementation outlined in Section 3.3[2]. Specifically, we developed a plug-in (Figure 4A) for *OnShape*[3] to embed and edit the mechanical components of the widgets on 3D models. Users can import solid models (i.e., *STEP*, *DWG* files) or design their own, and specify the widget type, location, and relevant dimensions on the model to 3D print. Additionally, we built a *Processing*[4] tool (Figure 4B) to design radial and linear patterns, preview the generated Moiré effect, and export the transparent and opaque layers at actual-size. Users may adjust the dimensions and line spacing distance for each layer and see an animation of the superimposed patterns. Finally, users can generate *PDF* or *DXF* files to print on paper to verify the desired dimensions and appearance.

Below, we identify critical design factors and summarize the key lessons learned during development which can guide users as they experiment with the design tools to create MoiréWidgets. These

---

[2]The source code for both tools can be found at https://github.com/dcz-xyz/MoireWidgets
[3]https://www.onshape.com/en/
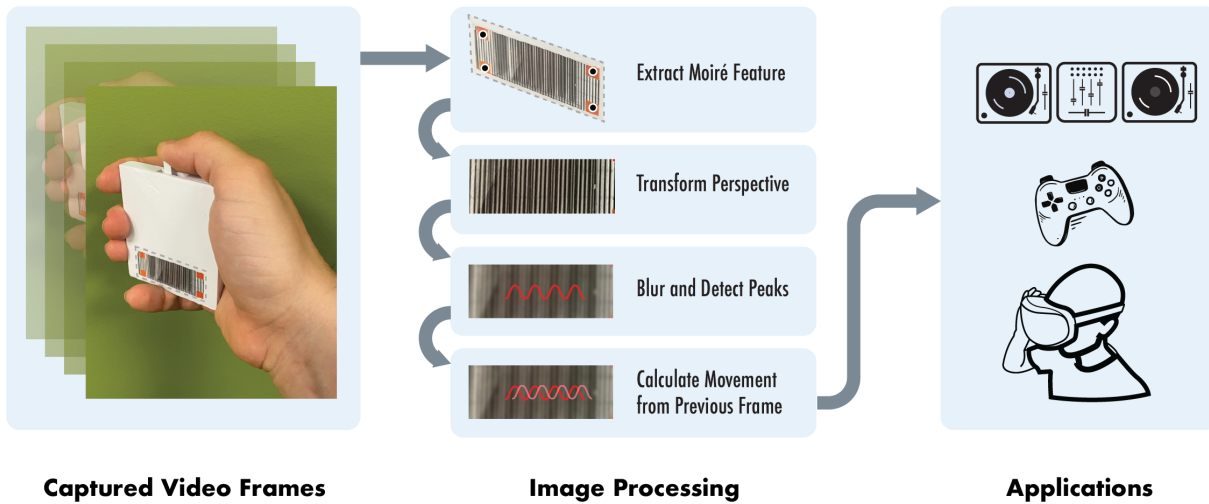[4]https://processing.org/

Figure 5: Our image processing pipeline takes captured video frames and extract the Moiré feature with the color markers at the corners. It crops out the rest of the image and applies a perspective transform. We then blur the Moiré fringes, detect the peaks in the visual signal, and calculate the displacement.

combined tools and insights offer a holistic approach to the design, implementation, and fabrication of Moiré-based widgets:

- *Signal Strength*: It is crucial to optimize the contrast between peaks in the Moiré feature (signal strength) by selecting an appropriate line thickness. Lines that are too thin (less than 0.2 mm) produce a weaker Moiré signal, while excessively thick lines result in overly dark patterns. We discovered that a line thickness ranging from 0.25 to 0.4 mm to be effective.

- *Aliasing*: The quality of the printer and its settings significantly affect the appearance of the Moiré pattern due to aliasing. This effect is particularly pronounced when printing radial lines spaced less than 3° apart.

- *Moiré Period*: Effective tracking can be achieved by a balance between the window size and the line spacing of each layer. For reliable tracking, we recommend that the tracking window contain at least three Moiré peaks.

3.5 Image Signal Processing

We utilize a similar image processing pipeline to those used in previous studies [38, 57] to convert visible alteration in the Moiré pattern into a displacement signal. According to the formulation in Section 3.1, the Moiré fringes can be represented as a sinusoidal function as $A\sin(wx + \phi) + B$. In previous studies that utilize the Moiré pattern for camera pose estimation, the pattern changes based on the camera angle and distance. However, given that our system minimizes the gap between the two stacked layers to generate the Moiré effect, we posit that the camera's position does not influence the pattern's appearance. This allows for the implementation of a simplified version of workflow to extract the Moiré signal.

We use *OpenCV* [6] for our image processing pipeline. An overview of the computation flow is presented in Figure 5. The first step in this process is to identify the area where the Moiré pattern is present. To achieve this, we place four colored square markers at the corners of the display window where the Moiré

pattern is present. Next, we apply a color threshold to separate the markers' masks, and locate their four inner corners. Since most of our prototypes are 3D printed with white material, we can isolate the Moiré pattern region without using complex detection mechanisms. Previous methods [57] have advocated for the use of fiducial markers to locate the Moiré pattern, a technique that remains applicable to our setup, especially if more complex textures are introduced to the widgets and the available space permits such installation.

Once the corners of the Moiré pattern region have been identified, we apply the `cv::warpPerspective` function to transform the identified region into a rectified view. This rectified view allows us to detect Moiré pattern changes in a standardized form regardless of the camera position. Given that the raw Moiré pattern exhibits numerous high-frequency components—a characteristic attributed to the impulse function-like nature of the stacked layer—we apply a Gaussian Blur filter following the conversion of the Moiré image to grayscale. The kernel size selected for the Gaussian Blur is equivalent to 10% of the rectified view's length. Subsequently, we calculate the average intensity along the y-axis of the blurred image, thereby generating a 1D intensity signal that can be utilized to estimate the Moiré displacement effectively.

Estimate Moiré Displacement. The estimation of Moiré displacement can be performed directly by fitting the previously derived 1D intensity signal with a sinusoidal function. First, we normalize the intensity signal to confine it within a range of -1 to 1. Then, we employ it to fit a sinusoidal function given by $f(x; A, B, \phi) = A\sin(wx + \phi) + B$. Here w is a constant and is determined by $w = 2\pi(T_a - T_b)/(T_a T_b)$, considering T_a and T_b are known values from the production time. Once the fitting is complete, the parameter ϕ, which is acquired during the fitting, can be leveraged to estimate the Moiré displacement. During the fitting process, we restrict A to be a positive value and ϕ in the range between 0 to 2π.

Daniel Campos Zamora, Mustafa Doga Dogan, Alexa Siu, Eunyee Koh, and Chang Xiao

Let us assume that ϕ_i represents the estimated phase from the i-th frame. The displacement Δx_i between frame i and frame $i - 1$ can be calculated using the equation

$$\Delta x_i = \frac{\Delta \phi T_m}{2\pi}, \tag{1}$$

where $\Delta \phi$ equals $\phi_i - \phi_{i-1}$, if $\phi_i \geq \phi_{i-1}$, or $\phi_i + 2\pi - \phi_{i-1}$ if $\phi_i < \phi_{i-1}$. We are assuming here that frames i and frame $i - 1$ are sufficiently close to each other, preventing the Moiré pattern from shifting by more than one period between the two frames.

This computational approach enables us to transform Moiré images into displacement signals, making them adaptable for controlling a wide array of applications. The precision of these displacement calculations has been thoroughly validated, demonstrating a high degree of accuracy in the experiments detailed in Section 4.

4 SYSTEM EVALUATION

In this section, we describe our apparatus and procedure to characterize MoiréWidgets' accuracy at different distances and viewing angles, and discuss the results.

4.1 Ground Truth and Baseline

We use the *Mitutoyo CD-6 ASX* high-precision caliper as the ground truth measurement for its precision of 0.012 mm ± 0.02 mm[5]. This precision is an order of magnitude higher compared to other camera-based tracking systems, such as the inside-out tracking system used in VR headsets (e.g., *SteamVR Base Station*[6], 0.56 mm ± 0.21 mm [2]) or the popular *OptiTrack*[7] (0.43 mm ± 0.17 mm [2]) motion capture system. Using a caliper makes our setup and data collection process easier because it gives direct number readings for each frame, which reliably measures the actual displacement and helps us accurately estimate the error in our system.

We also compare our system with the ArUco markers [13], a standard fiducial marker for location tracking. Originally designed for AR applications, ArUco markers have been widely used as ground truth or baseline in estimating object locations in the fields of robotics and computer vision [34, 49]. Additionally, both ArUco and our system serve as passive tags, have a similar physical size, and have the same hardware requirements that rely solely on an RGB camera for estimating displacement. Thus, comparing our system with ArUco can demonstrate our advantages as low-cost and passive visual tags for displacement measurement.

4.2 Evaluation Setup

We fabricated a fixture to secure one jaw of the high-precision digital caliper and allowed the other jaw to move along a linear path on laser-cut guide rails. A 3D printed carriage was interlocked with the moving jaw, and this carriage had ArUco markers and a Moiré window attached to it. The Moiré window slides over a bottom layer of a line pattern on the fixture, as illustrated in Figure 6A. The Moiré window and ArUco are roughly 3 by 3 cm. Such a configuration allows the Moiré window and ArUco markers to move in tandem with the moving jaw of the caliper, ensuring
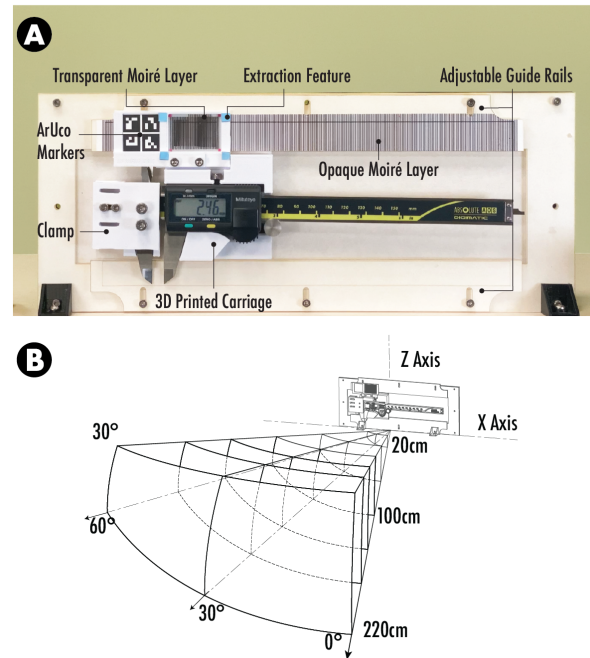
Figure 6: (A) The custom fixture that fastened the ArUco markers and Moiré fringes to digital calipers and slid along laser-cut guide rails. (B) Diagram showing the distances ranging from 20 cm to 220 cm and viewing angles ranging up to 60° in the X axis and 30° in the Z axis we used to characterize our performance.

that the caliper readings accurately reflect the precise displacement of our evaluation target.

For each camera setting, we reset the caliper to its starting position and manually moved the 3D printed carriage by up to 20 mm using the caliper's thumbscrew. The camera was positioned at a specific distance and angle, and we recorded a video of this movement. We extracted 25 evenly spaced frames to calculate displacement for each video. We varied the distance and angle of the camera, covering a range of 20 to 220 cm and capturing videos at up to 30° and 60° angles along the Z and X axes, respectively, to ensure a comprehensive evaluation. However, a combination of 30° / 60° in Z / X axes was excluded due to the extremity of the camera angle. All recordings were in 1080p and made using an *iPhone 11 Pro* mounted on a tripod. Figure 6B illustrates the range of distances and camera angles included in our evaluation.

We utilized the ArUco module [13] from *OpenCV* [6] to determine the ArUco displacement. We extracted the positions of the ArUco markers. Then, we use *OpenCV*'s camera calibration module to estimate the displacement. The Moiré pattern's displacement was tracked using our method, as described in Section 3.5. Both the ArUco and our method's estimations were rescaled to match the physical unit in millimeters.

4.3 Results

We computed the displacement estimation from both the ArUco and Moiré patterns, and used the caliper readings as the ground truth for calculating the error in millimeters for each method. The results are displayed in Figure 7. Each plot shows the Root Mean
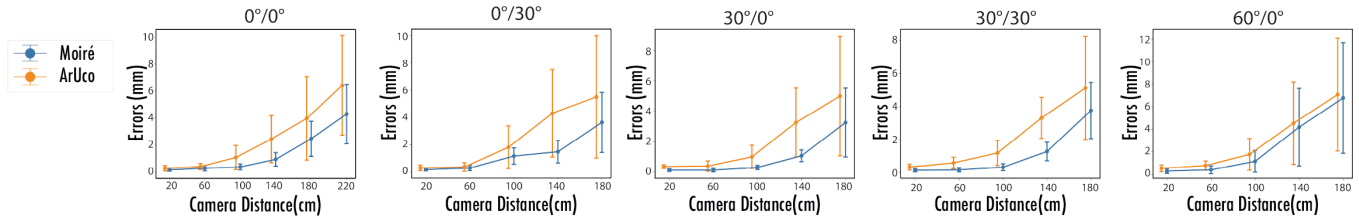
Figure 7: The results of our evaluation. Each plot represents the results at a specific camera angle (X°/Z°) with respect to distance changes in _cm_. The line segments show the RMSE measurement in _mm_, and the bars indicate the standard deviation of the error. Both our method and ArUco were measured under the same conditions. The ArUco plot is slightly shifted to the left for a clearer comparative visualization.

Square Errors (RMSE) at a fixed viewing angle and how they change with distance. The error is measured by $RMSE = \sqrt{\sum(X_i - \hat{X}_i)^2/n}$, where X_i is the estimated displacement from either our method or ArUco, and $\hat{X}_i$ is the digital reading from the caliper. n is the total number frames used for evaluation in one video recording. The standard deviation is computed by $\sqrt{\sum(X_i - \hat{X}_i - e)^2/n}$, where e represents the mean error across a single video recording session.

According to the results, both our method and ArUco demonstrate good accuracy (i.e., at the sub-millimeter level) when the camera is positioned at a close proximity of less than 60 cm to the target, with our method exhibiting slightly better accuracy. However, as the camera distance increases, ArUco shows larger errors compared to our method. Particularly at a distance of 140 cm and with a camera angle of 30°, ArUco displays errors of 2 to 4 mm and higher standard deviations of 1.5 to 3 mm, compared to closer distances. Meanwhile, our method continues to maintain a sub-millimeter accuracy, with 0.39 to 0.83 mm standard deviation. When the camera angle is increased to 60° and distance is larger than 140 cm, both our method and ArUco exhibit a high level of error (greater than 4.0 mm ± 3.5 mm), suggesting that a narrower camera angle is preferable in practical applications.

We have also conducted a significance test using the paired t-test to examine all conditions in comparison between our method and ArUco. This analysis evaluated the RMSE and its standard deviation, operating under the null hypothesis that there is no significant difference in RMSE/standard deviation between our method and ArUco. The results, $p_{\text{RMSE}} = 6.13 \times 10^{-6}$ and $p_{\text{std}} = 3.74 \times 10^{-5}$, demonstrate that both the RMSE and its standard deviation are significantly smaller with our method compared to ArUco ($p < 0.001$). It is also worth noting that in the context of marker tracking, the worst-case performance holds greater practical importance than average performance, particularly in scenarios characterized by large variances (as observed with ArUco in Figure 7). Our method outperforms ArUco in terms of average error and exhibits a much smaller standard deviation, which indicates better robustness.

We observed that as the distance increases to 180 cm, our method begins to show decreased performance, evidenced by an increase in both the RMSE and the standard deviation, surpassing 3.2 mm ± 2.2 mm. Also, the error increases as the camera angle becomes wider. Such increase in error metrics potentially leads to unreliable tracking performance. A high RMSE may cause incorrect cursor location estimation for widgets like sliders. Similarly, a high standard deviation can lead to fluctuations in tracking for widgets like push buttons. To illustrate, consider a 3 cm slider widget; a 3 mm error or standard deviation represents a substantial 10% error in location estimation or a 10% fluctuation in tracking. Consequently, we recommend maintaining the widgets within a 140 cm operating range and at an angle of less than 30° relative to the camera. This range is suitable for HMD-type applications, such as when a user wears AR glasses and uses MoiréWidgets to send control signals to the camera on the glasses (e.g., Figure 8). Since these widgets are operated by hand, the distance between the camera and the widgets will typically be within arm's reach, usually less than 100 cm.

5 DISCUSSION

In this section, we delve into the broader implications of our work and discuss its applications and potential areas for further exploration and improvement.

5.1 Applications

We demonstrate our approach MoiréWidgets by recreating a common example tangible interface and physical controller often used in TUI research. Specifically, we combine the button, dial, and slider to make an audio console that controls can toggle a play button and change the playback speed and volume of a song. (Figure 8. Our image processing pipeline sends OSC messages to a Max/MSP[8] program that decomposes the message and routes displacement value to the corresponding music control. In the future, this can be extended to other domains that benefit from passive, precise tangible interfaces. For example, in AR/VR, MoiréWidgets could take advantage of the built-in cameras of the headsets to enhance interactions with tangible peripherals. In robotics, where precision is crucial, MoiréWidgets could be used in remote controls to accurately move and position robots [24]. In digital art and design, they could empower designers to prototype and create interactive installations, opening avenues for engaging art experiences. Data visualizations also benefit from tangible user interfaces [4] and MoiréWidgets could offer researchers and professionals to explore complex datasets and graphics.

5.2 Limitations

Occlusion is an important consideration for any vision-based approach, including ours. If the visual feature is partially or entirely blocked by another object or the user's hand, detection accuracy

---

[8]https://cycling74.com/products/max

Figure 8: We integrate multiple widgets to create an audio console that controls a music interface that can be used for AR.

Figure 9: (A) The FDM sample shows and inconsistent fringe spacing and also warping. (B) The SLA object has support structures bonded to the Moiré fringes which are difficult to remove and cause significant warping and distortions.

may be compromised or completely fail. This is a fundamental limitation shared with other vision-based systems, such as ArUco and OptiTrack. Addressing occlusion is a complex task that warrants further investigation. One possible solution is to employ multiple cameras to capture a comprehensive view of a widget from different angles, or to introduce redundancy by having multiple Moiré windows that follow the same movement but are situated at different locations, thus reducing the likelihood of obstruction In our current implementation, we follow the practice of not positioning the Moiré window between the interaction point and the camera, thereby avoiding critical occlusion issues in our prototypes.

In our current implementation, we must assemble the FDM-printed mechanisms and Moiré paper patterns, primarily due the higher printing resolution, e.g., a standard paper printer's resolution of 300DPI is equivalent to 0.08 mm. In our early prototype, we attempted a fully 3D printed version that incorporated Moiré patterns directly into the structure, but the result was unsatisfactory. The Moiré patterns are warped and irregular (Figure 9A) so the necessary attributes required for displacement estimation cannot be reliably extracted. Stereolithography (SLA) 3D printers have support structures that bond to and damage the fringes (Figure 9B) and UV-cured resin printing—including digital light projection—lacks the ability to do multi-color prints. More sophisticated 3D printing methods like Polyjet and digital light synthesis (DLS) can also provide higher-resolution but their substantial cost but their substantial costs make them inaccessible to most users. In the future, advancements in 3D printing technologies could allow for a unified fabrication process. As higher-resolution 3D printers become more accessible, it becomes more practical to fabricate the entire widget, including the Moiré patterns, as a single entity.

Lastly, our method to extract and process the Moiré pattern can be improved by using more advanced computer vision algorithms. The four colored markers at the corners of the printed fringes used to extract and process the Moiré pattern can fail under irregular lighting conditions, like dark shadows and bright highlights, or when the printed widgets themselves exhibit a complex texture. We plan to explore improved detection and extraction algorithms that could, for example, leverage machine learning to recognize the Moiré features in various conditions.
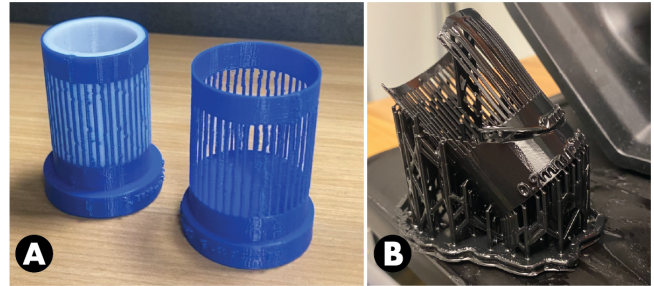
5.3 Design and Aesthetics

While our focus has primarily been on the functional aspects necessary for interaction, future iterations of MoiréWidget could explore the design of the patterns and overall aesthetics of the widgets. The Moiré effect has been studied with various geometries—dots [15] and hexagonal meshes [44]—and colors [9] that could expand the design possibilities for MoiréWidgets. This could impact users' perceptions of the widgets beyond just their functionality but also by their visual attractiveness and how well they blend into various contexts. In addition, we plan on expand our design tools to lets users experiment with different Moiré pattern designs, color palettes, and materials to create widgets that are both functional and aesthetically pleasing.

6 CONCLUSION

In this paper, we have introduced MoiréWidgets, a novel approach to high-precision passive tangible interaction through the utilization of the Moiré effect. By integrating Moiré patterns into 3D printed interactive mechanisms, we demonstrated a novel system for achieving fine-grained control for various interactions. Through a series of tests, we have shown that MoiréWidgets are more accurate and robust than standard fiducial markers. We demonstrate a sample application for audio mixing, and indicate how they could be extended to other applications like AR/VR, robotics, and data visualization. Future research could refine this technique by streamlining the fabrication process, improving the Moiré feature extraction, and exploring other aesthetic dimensions of the widgets. As HCI researchers continue to explore battery-free, passive devices, MoiréWidgets enables new possibilities for tangible interaction.

REFERENCES

[1] Marwa Alalawi, Noah Pacik-Nelson, Junyi Zhu, Ben Greenspan, Andrew Doan, Brandon M Wong, Benjamin Owen-Block, Shanti Kaylene Mickens, Wilhelm Jacobus Schoeman, Michael Wessely, Andreea Danielescu, and Stefanie Mueller. 2023. MechSense: A Design and Fabrication Pipeline for Integrating Rotary Encoders into 3D Printed Mechanisms. In *Proceedings of the 2023 CHI Conference on Human Factors in Computing Systems*. ACM, Hamburg Germany, 1–14. https://doi.org/10.1145/3544548.3581361

[2] Tim Ameler, Michaela Warzecha, Daniel Hes, Johannes Fromke, Annette Schmitz-Stolbrink, Christoph M. Friedrich, Kai Blohme, Lilith Brandt, Raphael Brungel, Alice Hensel, Lisa Huber, Francis Kuper, Jessica Swoboda, and Maren Warnecke. 2019. A Comparative Evaluation of SteamVR Tracking and the OptiTrack System for Medical Device Tracking. In *2019 41st Annual International Conference of the IEEE Engineering in Medicine and Biology Society (EMBC)*. IEEE, Berlin, Germany, 1465–1470. https://doi.org/10.1109/EMBC.2019.8856992

[3] J. A. Arriaga-Hernández and A. Jaramillo-Núñez. 2018. Ronchi and Moiré patterns for testing spherical and aspherical surfaces using deflectometry. *Applied Optics* 57, 34 (Dec. 2018), 9963. https://doi.org/10.1364/AO.57.009963

[4] S. Sandra Bae, Clement Zheng, Mary Etta West, Ellen Yi-Luen Do, Samuel Huron, and Danielle Albers Szafir. 2022. Making Data Tangible: A Cross-disciplinary Design Space for Data Physicalization. In *CHI Conference on Human Factors in Computing Systems*. ACM, New Orleans LA USA, 1–18. https://doi.org/10.1145/3491102.3501939

[5] Rafael Ballagas, Sarthak Ghosh, and James Landay. 2018. The Design Space of 3D Printable Interactivity. *Proceedings of the ACM on Interactive, Mobile, Wearable and Ubiquitous Technologies* 2, 2 (July 2018), 1–21. https://doi.org/10.1145/3214264

[6] Gary Bradski. 2000. The OpenCV Library. *Dr. Dobb's Journal of Software Tools* (2000).

[7] Jesse Burstyn, Nicholas Fellion, Paul Strohmeier, and Roel Vertegaal. 2015. Print-Put: Resistive and Capacitive Input Widgets for Interactive 3D Prints. In *Human-Computer Interaction – INTERACT 2015*, Julio Abascal, Simone Barbosa, Mirko Fetter, Tom Gross, Philippe Palanque, and Marco Winckler (Eds.). Vol. 9296. Springer International Publishing, Cham, 332–339. https://doi.org/10.1007/978-3-319-22701-6_25 Series Title: Lecture Notes in Computer Science.

[8] Moritz Bächer, Benjamin Hepp, Fabrizio Pece, Paul G. Kry, Bernd Bickel, Bernhard Thomaszewski, and Otmar Hilliges. 2016. DefSense: Computational Design of Customized Deformable Input Devices. In *Proceedings of the 2016 CHI Conference on Human Factors in Computing Systems*. ACM, San Jose California USA, 3806–3816. https://doi.org/10.1145/2858036.2858354

[9] Robert Czarnek. 1986. Moire Interferometry With Chromatic 1ight. In *Current Developments in Optical Engineering and Diffraction Phenomena*, Robert E. Fischer, James E. Harvey, and Warren J. Smith (Eds.), Vol. 0679. SPIE, 157 – 164. https://doi.org/10.1117/12.939581 Backup Publisher: International Society for Optics and Photonics.

[10] Mustafa Doga Dogan, Raul Garcia-Martin, Patrick William Haertel, Jamison John O'Keefe, Ahmad Taka, Akarsh Aurora, Raul Sanchez-Reillo, and Stefanie Mueller. 2023. BrightMarker: 3D Printed Fluorescent Markers for Object Tracking. In *36th Annual ACM Symposium on User Interface Software and Technology (UIST '23)*. ACM, San Francisco, CA. https://doi.org/10.1145/3586183

[11] Mustafa Doga Dogan, Ahmad Taka, Michael Lu, Yunyi Zhu, Akshat Kumar, Aakar Gupta, and Stefanie Mueller. 2022. InfraredTags: Embedding Invisible AR Markers and Barcodes Using Low-Cost, Infrared-Based 3D Printing and Imaging Tools. In *Proceedings of the 2022 CHI Conference on Human Factors in Computing Systems*. Association for Computing Machinery, New Orleans LA USA, 9. https://doi.org/10.1145/3491102.3501951

[12] Ramon Estana and Heinz Woern. 2003. Moiré-based positioning system for microrobots. In *Optical Measurement Systems for Industrial Inspection III*, Wolfgang Osten, Malgorzata Kujawinska, and Katherine Creath (Eds.), Vol. 5144. SPIE, 431 – 442. https://doi.org/10.1117/12.499920 Backup Publisher: International Society for Optics and Photonics.

[13] S. Garrido-Jurado, R. Muñoz-Salinas, F.J. Madrid-Cuevas, and M.J. Marín-Jiménez. 2014. Automatic generation and detection of highly reliable fiducial markers under occlusion. *Pattern Recognition* 47, 6 (June 2014), 2280–2292. https://doi.org/10.1016/j.patcog.2014.01.005

[14] Christopher Getschmann and Florian Echtler. 2021. Seedmarkers: Embeddable Markers for Physical Objects. In *Proceedings of the Fifteenth International Conference on Tangible, Embedded, and Embodied Interaction (TEI '21)*. Association for Computing Machinery, New York, NY, USA, 1–11. https://doi.org/10.1145/3430524.3440645

[15] Leon Glass. 1969. Moiré Effect from Random Dots. *Nature* 223, 5206 (Aug. 1969), 578–580. https://doi.org/10.1038/223578a0

[16] Jun Gong, Olivia Seow, Cedric Honnet, Jack Forman, and Stefanie Mueller. 2021. MetaSense: Integrating Sensing Capabilities into Mechanical Metamaterial. In *The 34th Annual ACM Symposium on User Interface Software and Technology*. ACM, Virtual Event USA, 1063–1073. https://doi.org/10.1145/3472749.3474806

[17] Peter Gyory, S. Sandra Bae, Ruhan Yang, Ellen Yi-Luen Do, and Clement Zheng. 2023. Marking Material Interactions with Computer Vision. In *Proceedings of the 2023 CHI Conference on Human Factors in Computing Systems*. ACM, Hamburg Germany, 1–17. https://doi.org/10.1145/3544548.3580643

[18] Timo Götzelmann and Daniel Schneider. 2016. CapCodes: Capacitive 3D Printable Identification and On-screen Tracking for Tangible Interaction. In *Proceedings of the 9th Nordic Conference on Human-Computer Interaction*. ACM, Gothenburg Sweden, 1–4. https://doi.org/10.1145/2971485.2971518

[19] Sebastian Günther, Martin Schmitz, Florian Müller, Jan Riemann, and Max Mühlhäuser. 2017. BYO*: Utilizing 3D Printed Tangible Tools for Interaction on Interactive Surfaces. In *Proceedings of the 2017 ACM Workshop on Interacting with Smart Objects*. ACM, Limassol Cyprus, 21–26. https://doi.org/10.1145/3038450.3038456

[20] Chris Harrison, Jason Wiese, and Anind Dey. 2010. Achieving Ubiquity: The New Third Wave. *Multimedia, IEEE* 17 (Oct. 2010), 8 – 12. https://doi.org/10.1109/MMUL.2010.53

[21] Liang He, Gierad Laput, Eric Brockmeyer, and Jon E. Froehlich. 2017. Squeeza-Pulse: Adding Interactive Input to Fabricated Objects Using Corrugated Tubes and Air Pulses. In *Proceedings of the Eleventh International Conference on Tangible, Embedded, and Embodied Interaction*. ACM, Yokohama Japan, 341–350. https://doi.org/10.1145/3024969.3024976

[22] Lars Erik Holmquist. 2023. Bits are Cheap, Atoms are Expensive: Critiquing the Turn Towards Tangibility in HCI. In *Extended Abstracts of the 2023 CHI Conference on Human Factors in Computing Systems*. ACM, Hamburg Germany, 1–8. https://doi.org/10.1145/3544549.3582744

[23] Eva Hornecker. 2011. The role of physicality in tangible and embodied interactions. *Interactions* 18, 2 (March 2011), 19–23. https://doi.org/10.1145/1925820.1925826

[24] Haiying Hu, Jiawei Li, Zongwu Xie, Bin Wang, Hong Liu, and G. Hirzinger. 2005. A robot arm/hand teleoperation system with telepresence and shared control. In *Proceedings, 2005 IEEE/ASME International Conference on Advanced Intelligent Mechatronics*. 1312–1317. https://doi.org/10.1109/AIM.2005.1511192

[25] Sungjae Hwang, Myungwook Ahn, and Kwang-yun Wohn. 2013. MagGetz: customizable passive tangible controllers on and around conventional mobile devices. In *Proceedings of the 26th annual ACM symposium on User interface software and technology*. ACM, St. Andrews Scotland, United Kingdom, 411–416. https://doi.org/10.1145/2501988.2501991

[26] Vikram Iyer, Justin Chan, Ian Culhane, Jennifer Mankoff, and Shyamnath Gollakota. 2018. Wireless Analytics for 3D Printed Objects. In *Proceedings of the 31st Annual ACM Symposium on User Interface Software and Technology*. ACM, Berlin Germany, 141–152. https://doi.org/10.1145/3242587.3242639

[27] Martin Kaltenbrunner and Ross Bencina. 2007. reacTIVision: a computer-vision framework for table-based tangible interaction. In *Proceedings of the 1st international conference on Tangible and embedded interaction*. ACM, Baton Rouge Louisiana, 69–74. https://doi.org/10.1145/1226969.1226983

[28] Scott R. Klemmer, Björn Hartmann, and Leila Takayama. 2006. How bodies matter: five themes for interaction design. In *Proceedings of the 6th conference on Designing Interactive systems*. ACM, University Park PA USA, 140–149. https://doi.org/10.1145/1142405.1142429

[29] Scott R. Klemmer, Jack Li, James Lin, and James A. Landay. 2004. Papier-Mache: Toolkit Support for Tangible Input. In *Proceedings of the SIGCHI Conference on Human Factors in Computing Systems (CHI '04)*. Association for Computing Machinery, New York, NY, USA, 399–406. https://doi.org/10.1145/985692.985743 event-place: Vienna, Austria.

[30] Gierad Laput, Eric Brockmeyer, Scott E. Hudson, and Chris Harrison. 2015. Acoustruments: Passive, Acoustically-Driven, Interactive Controls for Handheld Devices. In *Proceedings of the 33rd Annual ACM Conference on Human Factors in Computing Systems (CHI '15)*. Association for Computing Machinery, New York, NY, USA, 2161–2170. https://doi.org/10.1145/2702123.2702414

[31] David Ledo, Fraser Anderson, Ryan Schmidt, Lora Oehlberg, Saul Greenberg, and Tovi Grossman. 2017. Pineal: Bringing Passive Objects to Life with Embedded Mobile Devices. In *Proceedings of the 2017 CHI Conference on Human Factors in Computing Systems*. ACM, Denver Colorado USA, 2583–2593. https://doi.org/10.1145/3025453.3025652

[32] Simon J. Leigh, Robert J. Bradley, Christopher P. Purssell, Duncan R. Billson, and David A. Hutchins. 2012. A Simple, Low-Cost Conductive Composite Material for 3D Printing of Electronic Sensors. *PLOS ONE* 7, 11 (Nov. 2012), 1–6. https://doi.org/10.1371/journal.pone.0049365 Publisher: Public Library of Science.

[33] Hanchuan Li, Eric Brockmeyer, Elizabeth J. Carter, Josh Fromm, Scott E. Hudson, Shwetak N. Patel, and Alanson Sample. 2016. PaperID: A Technique for Drawing Functional Battery-Free Wireless Interfaces on Paper. In *Proceedings of the 2016 CHI Conference on Human Factors in Computing Systems*. ACM, San Jose California USA, 5885–5896. https://doi.org/10.1145/2858036.2858249

[34] Xiaohe Ma, Xianmin Xu, Leyao Zhang, Kun Zhou, and Hongzhi Wu. 2023. OpenSVBRDF: A Database of Measured Spatially-Varying Reflectance. *ACM Transactions on Graphics* 42, 6 (Dec. 2023), 1–14. https://doi.org/10.1145/3618358

[35] Edwin Olson. 2011. AprilTag: A robust and flexible visual fiducial system. In *2011 IEEE International Conference on Robotics and Automation*. 3400–3407. https://doi.org/10.1109/ICRA.2011.5979561 ISSN: 1050-4729.

[36] Gerald Oster, Mark Wasserman, and Craig Zwerling. 1964. Theoretical Interpretation of Moiré Patterns. *J. Opt. Soc. Am.* 54, 2 (Feb. 1964), 169–175. https://doi.org/10.1364/JOSA.54.000169 Publisher: Optica Publishing Group.

[37] Hao Peng, Peiqing Liu, Lin Lu, Andrei Sharf, Lin Liu, Dani Lischinski, and Baoquan Chen. 2020. Fabricable Unobtrusive 3D-QR-Codes with Directional Light. *Computer Graphics Forum* 39, 5 (Aug. 2020), 15–27. https://doi.org/10.1111/cgf.14065

[38] Simeng Qiu, Hadi Amata, and Wolfgang Heidrich. 2023. MoiréTag: Angular Measurement and Tracking with a Passive Marker. In *Special Interest Group on Computer Graphics and Interactive Techniques Conference Conference Proceedings*. ACM, Los Angeles CA USA, 1–10. https://doi.org/10.1145/3588432.3591538

[39] Gabriel Reyes, Jason Wu, Nikita Juneja, Maxim Goldshtein, W. Keith Edwards, Gregory D. Abowd, and Thad Starner. 2018. SynchroWatch: One-Handed Synchronous Smartwatch Gestures Using Correlation and Magnetic Sensing. *Proceedings of the ACM on Interactive, Mobile, Wearable and Ubiquitous Technologies* 1, 4 (Jan. 2018), 1–26. https://doi.org/10.1145/3161162

[40] Francisco Romero-Ramirez, Rafael Muñoz-Salinas, and Rafael Medina-Carnicer. 2018. Speeded Up Detection of Squared Fiducial Markers. *Image and Vision Computing* 76 (June 2018). https://doi.org/10.1016/j.imavis.2018.05.004

[41] Valkyrie Savage, Colin Chang, and Björn Hartmann. 2013. Sauron: embedded single-camera sensing of printed physical user interfaces. In *Proceedings of the 26th annual ACM symposium on User interface software and technology*. ACM, St. Andrews Scotland, United Kingdom, 447–456. https://doi.org/10.1145/2501988.2501992

[42] Valkyrie Savage, Andrew Head, Björn Hartmann, Dan B. Goldman, Gautham Mysore, and Wilmot Li. 2015. Lamello: Passive Acoustic Sensing for Tangible Input Components. In *Proceedings of the 33rd Annual ACM Conference on Human Factors in Computing Systems*. ACM, Seoul Republic of Korea, 1277–1280. https://doi.org/10.1145/2702123.2702207

[43] Valkyrie Savage, Carlos Tejada, Mengyu Zhong, Raf Ramakers, Daniel Ashbrook, and Hyunyoung Kim. 2022. AirLogic: Embedding Pneumatic Computation and I/O in 3D Models to Fabricate Electronics-Free Interactive Objects. In *Proceedings of the 35th Annual ACM Symposium on User Interface Software and Technology*. ACM, Bend OR USA, 1–12. https://doi.org/10.1145/3526113.3545642

[44] Vladimir Saveljev. 2016. Moiré effect in cylindrical objects. *Journal of the Korean Physical Society* 68, 9 (May 2016), 1075–1082. https://doi.org/10.3938/jkps.68.1075

[45] Vladimir Saveljev and Irina Palchikova. [n. d.]. Theory and computer simulation of the moiré patterns in single-layer cylindrical particles. ([n. d.]).

[46] Cassandra Scheirer and Chris Harrison. 2022. DynaTags: Low-Cost Fiducial Marker Mechanisms. In *Proceedings of the 2022 International Conference on Multimodal Interaction (ICMI '22)*. Association for Computing Machinery, New York, NY, USA, 432–443. https://doi.org/10.1145/3536221.3556591

[47] Martin Schmitz, Mohammadreza Khalilbeigi, Matthias Balwierz, Roman Lissermann, Max Mühlhäuser, and Jürgen Steimle. 2015. Capricate: A Fabrication Pipeline to Design and 3D Print Capacitive Touch Sensors for Interactive Objects. In *Proceedings of the 28th Annual ACM Symposium on User Interface Software & Technology (UIST '15)*. Association for Computing Machinery, New York, NY, USA, 253–258. https://doi.org/10.1145/2807442.2807503

[48] Martin Schmitz, Jürgen Steimle, Jochen Huber, Niloofar Dezfuli, and Max Mühlhäuser. 2017. Flexibles: Deformation-Aware 3D-Printed Tangibles for Capacitive Touchscreens. In *Proceedings of the 2017 CHI Conference on Human Factors in Computing Systems (CHI '17)*. Association for Computing Machinery, New York, NY, USA, 1001–1014. https://doi.org/10.1145/3025453.3025663

[49] Bugra Can Sefercik and Baris Akgun. 2023. Learning Markerless Robot-Depth Camera Calibration and End-Effector Pose Estimation. In *Proceedings of The 6th Conference on Robot Learning (Proceedings of Machine Learning Research, Vol. 205)*, Karen Liu, Dana Kulic, and Jeff Ichnowski (Eds.). PMLR, 1586–1595. https://proceedings.mlr.press/v205/sefercik23a.html

[50] Lei Shi, Holly Lawson, Zhuohao Zhang, and Shiri Azenkot. 2019. Designing Interactive 3D Printed Models with Teachers of the Visually Impaired. In *Proceedings of the 2019 CHI Conference on Human Factors in Computing Systems*. ACM, Glasgow Scotland Uk, 1–14. https://doi.org/10.1145/3290605.3300427

[51] Lei Shi, Ross McLachlan, Yuhang Zhao, and Shiri Azenkot. 2016. Magic Touch: Interacting with 3D Printed Graphics. In *Proceedings of the 18th International ACM SIGACCESS Conference on Computers and Accessibility (ASSETS '16)*. Association for Computing Machinery, New York, NY, USA, 329–330. https://doi.org/10.1145/2982142.2982153

[52] Paul Streli, Rayan Armani, Yi Fei Cheng, and Christian Holz. 2023. HOOV: Hand Out-Of-View Tracking for Proprioceptive Interaction using Inertial Sensing. In *Proceedings of the 2023 CHI Conference on Human Factors in Computing Systems*. ACM, Hamburg Germany, 1–16. https://doi.org/10.1145/3544548.3581468

[53] Aaron Visschedijk, Hyunyoung Kim, Carlos Tejada, and Daniel Ashbrook. 2022. ClipWidgets: 3D-printed Modular Tangible UI Extensions for Smartphones. In *Sixteenth International Conference on Tangible, Embedded, and Embodied Interaction*. ACM, Daejeon Republic of Korea, 1–11. https://doi.org/10.1145/3490149.3501314

[54] Malte Weiss, Julie Wagner, Yvonne Jansen, Roger Jennings, Ramsin Khoshabeh, James D Hollan, and Jan Borchers. 2009. SLAP Widgets: Bridging the Gap Between Virtual and Physical Controls on Tabletops. (2009).

[55] Jian Wu, Ting-ting Zhou, Bo Yuan, and Li-qiang Wang. 2016. A digital moiré fringe method for displacement sensors. *Frontiers of Information Technology & Electronic Engineering* 17, 9 (Sept. 2016), 946–953. https://doi.org/10.1631/FITEE.1500270

[56] Chang Xiao, Karl Bayer, Changxi Zheng, and Shree K. Nayar. 2019. Vidgets: modular mechanical widgets for mobile devices. *ACM Transactions on Graphics* 38, 4 (Aug. 2019), 1–12. https://doi.org/10.1145/3306346.3322943

[57] Chang Xiao and Changxi Zheng. 2021. MoiréBoard: A Stable, Accurate and Low-cost Camera Tracking Method. In *The 34th Annual ACM Symposium on User Interface Software and Technology*. ACM, Virtual Event USA, 881–893. https://doi.org/10.1145/3472749.3474793

[58] Peiyu Zhang, Wen Ying, and Seongkook Heo. 2022. Fringer: A Finger-Worn Passive Device Enabling Computer Vision Based Force Sensing Using Moiré Fringes. In *The Adjunct Publication of the 35th Annual ACM Symposium on User Interface Software and Technology*. ACM, Bend OR USA, 1–3. https://doi.org/10.1145/3526114.3558706

[59] Clement Zheng, Peter Gyory, and Ellen Yi-Luen Do. 2020. Tangible Interfaces with Printed Paper Markers. In *Proceedings of the 2020 ACM Designing Interactive Systems Conference*. ACM, Eindhoven Netherlands, 909–923. https://doi.org/10.1145/3357236.3395578